

# Forecasts for a mm sky survey of the Northern Hemisphere with a 13-m antenna

M. Fernández-Torreiro<sup>1,\*</sup>, J. F. Macías-Pérez<sup>1</sup>, D. Chérouvrier<sup>1</sup>, and F. X. Désert<sup>2</sup>

<sup>1</sup>Laboratoire de Physique Subatomique et de Cosmologie, Université Grenoble Alpes, CNRS/IN2P3, 53 Avenue des Martyrs, Grenoble, France

<sup>2</sup>Univ. Grenoble Alpes, CNRS, IPAG, F-38000 Grenoble, France

**Abstract.** Most of the cosmic microwave background instruments currently observing at mm wavelengths are located in the Southern Hemisphere, and those in the Northern one are focused on observations of the large scale anisotropies with small aperture telescopes. Therefore, there is a gap for an instrument with a large mirror ( $D \geq 10$  m) that would survey the Northern sky. We propose a new photometer to be placed on a 13-meter diameter antenna in the Northern Hemisphere, which would observe the sky with four different bands: 90, 150, 220 and 260 GHz (3, 2, 1.4 and 1.15 mm, respectively) with  $\leq 1'$  resolution and a field-of-view of 1 deg. We present a new set of simulations to assess the capabilities of the instrument when performing blind systematic detections of galaxy clusters through their Sunyaev-Zel'dovich effect signal. We consider a wide and a deep survey covering 6000 and 300 deg<sup>2</sup> (named WS and DS, respectively) and observing for 3 years each with 50% time efficiency. We present the expected number of detections in both scenarios, and compare them with previous similar surveys.

## 1 Introduction

In this paper we propose a new, 10-m class instrument observing at mm wavelengths, that would run blind searches of galaxy clusters through their Sunyaev-Zel'dovich effect counterparts [1]. Such instrument would be placed in the Northern Hemisphere to complement those that observed (e.g. the Atacama Cosmology Telescope [ACT, 2, 3]), are observing (e.g. the South Pole Telescope [SPT, 4]) or are planned to observe (most importantly the Simons Observatory, SO [5], especially through its large aperture telescopes -LAT- [6]) in the Southern Hemisphere. A possible location would be the Teide Observatory, in Tenerife (Spain), located at latitude  $+28^\circ$  and 2400 meters of altitude, on a 13-m antenna. The instrument would have four frequency bands at 90, 150, 220 and 260 GHz and a field-of-view (FoV) of 1 deg, with more than 70k kinetic inductance detectors (KIDs) in total. The CNRS has a long and proven record of developing such array detectors [7–9].

We generated realistic simulations of mm sky maps with systematics consistent with those from NIKA2 [7], a previous KID mm photometer located at 2850 m of altitude in Pico Veleta, Granada, Spain. In Section 2 we present the different emission components that were taken into account in these maps, together with a description of the expected noise and filtering,

---

\*mateo@fernandeztorreiro.com

**Table 1.** Summary of the astrophysical components and instrumental effects considered in the output simulations. The latter have been estimated from real data obtained by the NIKA2 instrument at the IRAM 30-m telescope, on top of which we added the expected improvement because of the different configuration (see text).

Component	Summary	Section
Galaxy clusters	Distribution from [11]	2.1
Cosmic Microwave Background	Power spectrum from ACT [2]	2.2
Synchrotron point sources	Random samples from [13]	2.3
Dust point sources	Realizations using SIDES [14, 15]	2.4
White and $1/f$ noise	Scaled from NIKA2 power spectra [10]	2.5
Realistic filtering	Transfer functions from NIKA2 [10]	2.6

based on previously published NIKA2 estimates [10]. In Section 3 we present how the cluster features were extracted from the frequency maps using a matched filter, and then matched against the input catalogue to discern between false and true detections. We also compare our matched sample to those from previous surveys. Finally, we conclude in Section 4.

## 2 Components of the simulated data

We produced  $N=1000$  realistic simulations of the sky signal, each with size  $2.5^\circ \times 2.5^\circ$ . We considered four astrophysical emission components, which are described in the following subsections. In addition, we explain the effect that the noise (statistical and instrumental) and the filtering from our experiment would have on the data. A summary of both is available in Table 1.

### 2.1 Galaxy cluster distribution

We randomly sampled the  $M_{500} - z$  distribution in [11] to populate our  $2.5^\circ \times 2.5^\circ$  fields. We sampled the distribution in 28 and 22 bins for  $2 \cdot 10^{13} < M_{500}(M_\odot) < 3 \cdot 10^{15}$  and  $0 < z < 3$  ranges, respectively. Once we had their distribution, we used the `minot` package [12] to integrate the SZ signal along the line-of-sight and recovered the  $Y$  map.

### 2.2 Cosmic microwave background anisotropies

We introduced a component accounting for cosmic microwave background (CMB) anisotropies. Although the filtering in the NIKA2 COSMOS data was too important to actually measure such anisotropies [10], one of the objectives of our work was to study the changes implied by a less aggressive filtering. We explored how the completeness and purity of the recovered sample changed with the filtering.

### 2.3 Synchrotron/radio point sources

We took the spectral index catalogue between 0.147–1.4 GHz from [13] and computed the source density for a  $2.5^\circ \times 2.5^\circ$  field. Then, we took random samples from the catalogue and placed them randomly on  $(x, y)$  positions in our simulations. Although the impact from radio point sources on the extraction of clusters is expected to be small, we kept them as the brightest ones could bias the feature extraction from the matched filter (see Section 3).

## 2.4 Dust point sources

We used the SIDES code [14, 15] to compute both the continuum and line emission components from dust point sources between 60 and 300 GHz. For this analysis, we only computed one  $2.5^\circ \times 2.5^\circ$  cube, then selected the spectral bins closer to the instrument observing frequencies and added them to our simulations. In Fig. 1 we show the maps of galaxy clusters, radio point sources and dust point sources.

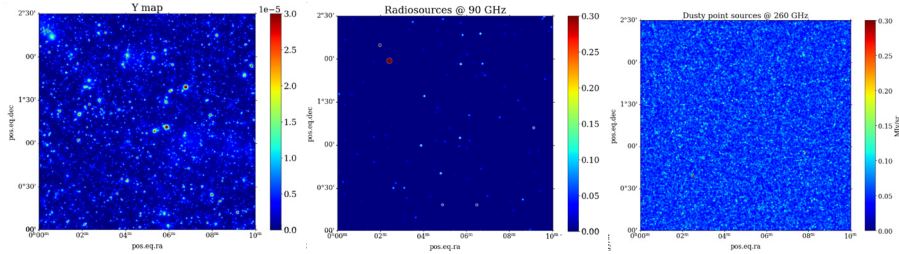


**Figure 1.** Maps of the astrophysical components considered in the simulations (excluding the CMB). From left to right: Y map from galaxy clusters, radio point sources, and dusty point sources.

## 2.5 White and $1/f$ noise components

We computed the power spectra from the jackknife maps for 2 and 1 mm data in [10], we show the former in Fig. 2. We fitted each one to a combination of white and  $1/f$  noise:

$$C(k) = C_w \left[ 1 + \left( \frac{k_k}{k} \right)^\alpha \right] \quad (1)$$

where  $C_w$  is the white noise level and  $k_k$  the knee frequency. We scaled both components by the improvement factors expected for each of the proposed surveys. In the case of the DS, which would cover  $300 \text{ deg}^2$  for 1.5 running years with a  $1^\circ$  FoV instead of NIKA2 COSMOS  $0.4 \text{ deg}^2$  for 180 hours with  $6.5'$  FoV, we expect a factor 4.8 improvement in the noise estimate. On the other hand, the WS would cover  $6000 \text{ deg}^2$  for the same amount of time, so we actually expect a worsening of the noise estimate by a factor 4.2.

## 2.6 Instrument filtering of the astrophysical data

Because of the limited extent of the FoV of the telescope, features larger than certain scales get cut from the data when recorded. The actual extent limit of these scales depends not only on the instrument characteristics, but also on its post-processing. In Fig. 2 we show the transfer function (TF; the transmitted signal as a function of scale) presented in [10] for the NIKA2 COSMOS data, and we compare it with two additional simulated transfer functions that we also applied to our simulations. In this way, we can repeat our analysis and study how the transfer function actually the detection of galaxy clusters. We fitted the NIKA2 TF to:

$$\text{TF}(k) = a - \frac{b}{k^c} \quad (2)$$

with  $a_0 = 1.04677 \pm 0.00073$ ,  $b_0 = 0.1850 \pm 0.0018$  and  $c_0 = 1.252 \pm 0.010$  best-fit values. For the other two cases, we assumed  $a = 1$  with  $b = (0.1, 0.01)b_0$  and  $c = (2, 4)c_0$ , respectively.

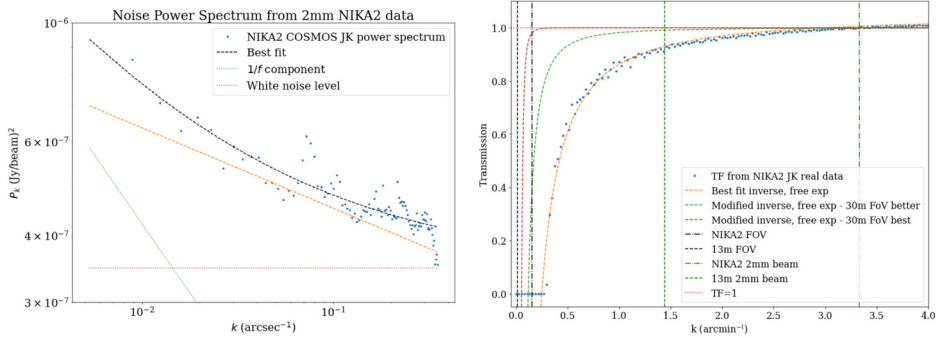


**Figure 2.** Left: noise power spectrum computed from the difference of 2 mm jackknife maps from [10]. We show the best fit values for both the white and  $1/f$  components. The sum of the two is the quantity actually used to build the noise maps added to our simulations, as in that way we neglected the maxima at higher  $k$ , coming from electronics. Right: three different transfer functions considered, labelled as NIKA2, “better” and “best”, from more to less important filtering at large scales (low  $k$ ). The values for bins with scales  $k < \text{FoV}^{-1}$  are fixed to 0.

### 3 Results & Discussion

In Fig. 3 we show the output of the simulation pipeline once all the components presented in the previous Section have been taken into account. We have plotted the case scenario with the TF equivalent to that from NIKA2, so the CMB anisotropies are clearly filtered out.

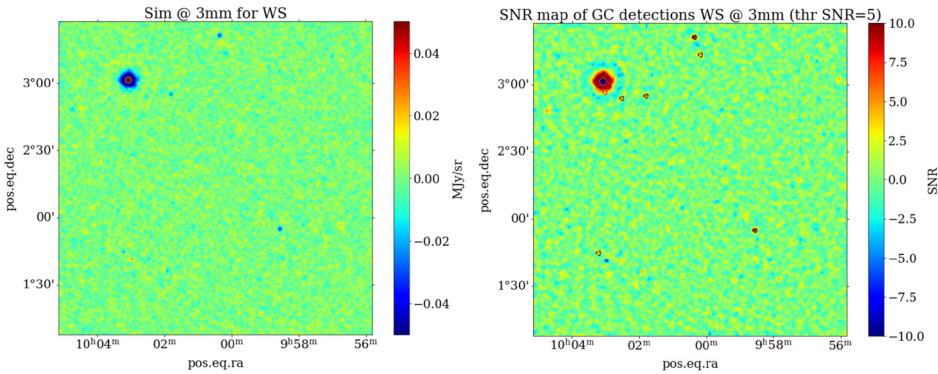


**Figure 3.** Left: one final simulation of a  $2.5^\circ \times 2.5^\circ$  field observed at 3 mm with the equivalent WS noise description. We can clearly see how the presence of a bright radio source towards the north-east has introduced a local minimum after the filtering of the data. Right: signal-to-noise ratio maps after running the matched filter, with a template size of  $60''$ , equivalent to 1 FWHM from the 13-m antenna 3 mm. The black circles are the detections used in the following analyses, while the red ones are discarded, as they clearly arise from the previous filtering issue.

Once the simulations are ready, we ran an improved version of the matched filter applied in [10]. We discard detections more than 1 FWHM away from the closest galaxy cluster in our catalogue (the one generated in Section 2.1), but also those that are too close to each other. We only kept a detection that is less than 3 FWHM away from another when any of the two account for more than 80% of the combined  $Y_{500}$  value from the catalogue. In this way,

we prevented spurious detections from entering the analysis, as it was shown in Fig. 3. We stored the mass and redshift values for the input clusters assigned to the detections left. We computed the purity curves for our catalogues and found a trend very similar to that described in [10], with purity surpassing 50% at signal-to-noise ratio, SNR, equal to 5.

We plot the  $M_{500} - z$  values for the detected clusters in Fig. 4. We also provide a comparison with those from existing SZ catalogues of galaxy clusters [e.g., 3, 4, 16] and also the detections in [10]. As expected, it is immediately clear how our distribution is better aligned with that from SPT<sup>1</sup> than that from NIKA2, because of the similar resolution with the former. The larger resolution of our instrument when compared to NIKA2 prevents us from resolving the emission from the most distant and compact clusters. We also recover a smaller amount of detections with smaller masses and lower redshift than the rest of wide surveys, probably because of the more important atmospheric noise contribution when compared to ACT or SPT. Our limiting transfer function at large scales also prevents the detection of the more diffuse clusters<sup>2</sup>. However, we acknowledge that some work is still to be done in the cleaning of the matching sample, as the two detections with  $z > 2.0$  in Fig. 4 are likely false.

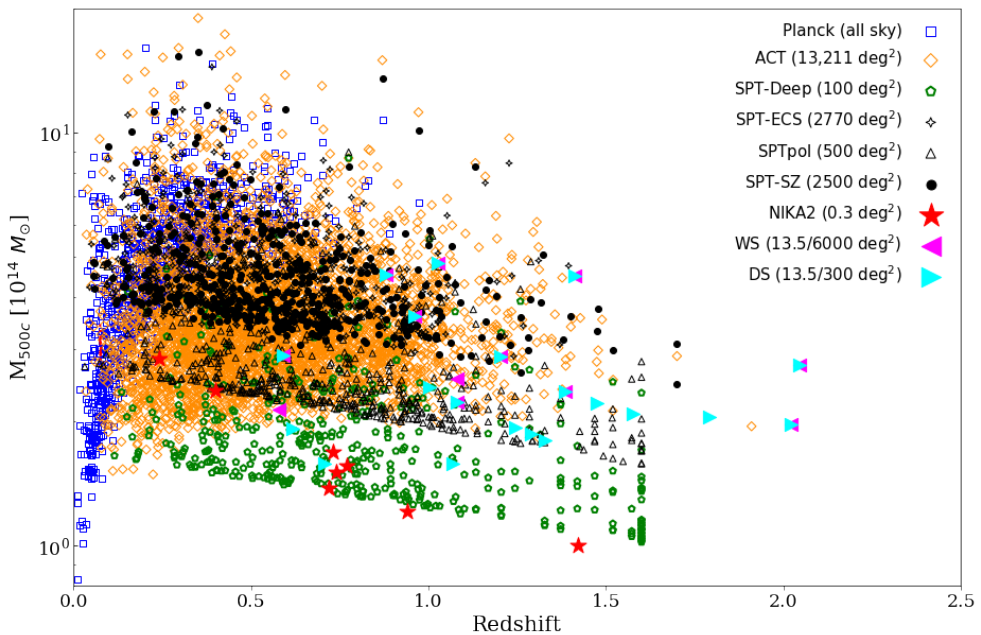


**Figure 4.** Our matched sample, limited to 3 simulations to prioritize legibility, both for the DS and WS and compared to legacy surveys. We see that our surveys trace slightly larger redshifts than previous ones, such as ACT or SPT-SZ. The Planck survey covers a different region of the sample at lower redshifts, due to its limited angular resolution. We see how most of the absent detections in the WS w.r.t. the DS are located at lower masses/higher redshifts, further proving the improved sensibility of the latter. Finally, we see an alignment between our surveys and results from SPTpol; the final goal of this work would be to provide a similar sample of clusters, for the first time in the Northern Hemisphere, down to  $M_{500} \sim 2 \cdot 10^{14}$  and up to  $z \sim 1 - 2$ .

<sup>1</sup>Except for the SPTdeep survey, which benefits not only from superb observing conditions but also from longer integration time.

<sup>2</sup>We leave the detailed discussion on the dependence of completeness with the transfer function for an upcoming work: we see small variations of the completeness of the matched samples.

## 4 Conclusions

After running the matched filter and discarding detections without a nearby cluster that could be responsible for the emission, we scaled the number to the areas of WS and DS (6000 and 300 deg<sup>2</sup>). We obtained a matched sample of more than 6000 and 400 clusters, respectively, for SNR $\geq$ 5. For this SNR we would obtain a similar purity to that achieved by NIKA2, around 50%. The completeness of the two surveys would differ, as the DS will detect more clusters with lower masses and higher redshifts. DS will achieve a similar performance to that of the SPTpol [4] sample: the slightly larger antenna diameter (13 m vs 10 m) would partly compensate the expected worse atmospheric noise when compared to the stable South Pole. The WS, on the other hand, would prove to be a valuable tool for modern cosmology and astrophysics, with a catalogue extent similar to that of ACT [3] at twice its resolution while almost certainly providing novel discoveries of clusters above declination  $\delta \geq 22^\circ$ .

## References

- [1] Sunyaev, R. A. & Zeldovich, Y. B. 1972, *Comments on Astrophysics and Space Physics*, 4, 173
- [2] Das, S., Louis, T., Nolta, M. R., *et al.* 2014, *JCAP*, 2014, 4, 014. doi:10.1088/1475-7516/2014/04/014
- [3] Hilton, M., Sifón, C., Naess, S., *et al.* 2021, *ApJS*, 253, 1, 3. doi:10.3847/1538-4365/abd023
- [4] Bleem, L. E., Klein, M., Abbot, T. M. C., *et al.* 2024, *The Open Journal of Astrophysics*, 7, 13. doi:10.21105/astro.2311.07512
- [5] Ade, P., Aguirre, J., Ahmed, Z., *et al.* 2019, *JCAP*, 2019, 2, 056. doi:10.1088/1475-7516/2019/02/056
- [6] Abitbol, M., Abril-Cabezas, I., Adachi, S., *et al.* 2025, *JCAP*, 2025, 8, 034. doi:10.1088/1475-7516/2025/08/034
- [7] Perotto, L., Ponthieu, N., Macías-Pérez, J. F., *et al.* 2020, *A&A*, 637, A71. doi:10.1051/0004-6361/201936220
- [8] CONCERTO Collaboration, Ade, P., Aravena, M., *et al.* 2020, *A&A*, 642, A60. doi:10.1051/0004-6361/202038456
- [9] Macías-Pérez, J. F., Fernández-Torreiro, M., Catalano, A., *et al.* 2024, *PASP*, 136, 11, 114505. doi:10.1088/1538-3873/ad8189
- [10] Chéroutrier, D., Macías-Pérez, J. F., Désert, F. X., *et al.* 2025, *A&A*, 700, A30. doi:10.1051/0004-6361/202554450
- [11] Tinker, J., Kravtsov, A. V., Klypin, A., *et al.* 2008, *ApJ*, 688, 2, 709. doi:10.1086/591439
- [12] Adam, R., Goksu, H., Leingärtner-Goth, A., *et al.* 2020, *A&A*, 644, A70. doi:10.1051/0004-6361/202039091
- [13] de Gasperin, F., Intema, H. T., & Frail, D. A. 2018, *MNRAS*, 474, 4, 5008. doi:10.1093/mnras/stx3125
- [14] Béthermin, M., Wu, H.-Y., Lagache, G., *et al.* 2017, *A&A*, 607, A89. doi:10.1051/0004-6361/201730866
- [15] Béthermin, M., Gkogkou, A., Van Cuyck, M., *et al.* 2022, *A&A*, 667, A156. doi:10.1051/0004-6361/202243888
- [16] Planck Collaboration, Ade, P. A. R., Aghanim, N., *et al.* 2016, *A&A*, 594, A27. doi:10.1051/0004-6361/201525823